PHYSICAL REVIEW B VOLUME 43, NUMBER 5 15 FEBRUARY 1991-I

First-principles molecular-dynamics simulation of liquid and amorphous selenium

D. Hohl* and R. O. Jones
Institut für Festkörperforschung, Forschungszentrum Jülich, D-5170 Jülich, Federal Republic of Germany
(Received 11 September 1990)

A molecular-dynamics simulation has been carried out for liquid and amorphous selenium in the temperature range 350–720 K. The simulation used 64 atoms in a constant-volume simple cubic cell, and the energy surfaces and forces were calculated using the density-functional formalism, with a local-density approximation for the exchange-correlation energy. The main focus is on the microscopic atomic structure, with the associated short- and intermediate-range ordering phenomena. Ring statistics, pair correlation functions $g(r)$, structure factors $S(Q)$, bond angle and dihedral angle distribution functions, phonon densities of states, and diffusion constants D were computed and compared with experimental and theoretical data where available. Several structural models proposed previously for Se are evaluated and their predictions compared with the results of the present simulation. Special emphasis is given to the concentration, structure, and stability of the dominant defects, and a structure and defect model is presented.

I. INTRODUCTION

Liquid (ℓ-Se) and amorphous or vitreous (a-Se) selenium[1] have been investigated extensively for more than half a century.[2,3] There are several reasons. First, apart from its group-VIA neighbor sulfur and the group-VA element phosphorus, selenium is the element with the most allotropes,[4] many of which are fascinating from a structural point of view. In addition to the various amorphous and vitreous forms, five crystalline modifications exist under normal pressure and temperature conditions: Trigonal ("metallic," "grey") t-Se, α-, β- and γ-monoclinic Se, and rhombohedral Se. Polymeric t-Se consists of parallel helical chains (space group $C3_121$ or $C3_221$, molecular point group D_3) and is thermodynamically stable at 300 K and 1.013 bars. The monoclinic and rhombohedral forms are molecular crystals with building blocks of Se_8 and Se_6, respectively. While other ring molecules ($Se_{5,7,9,10}$) and smaller clusters (Se_3,Se_4) have been synthesized chemically, identified in the gas phase, or both, the structures are poorly characterized.[5] Table I shows that all condensed forms of Se have twofold nearest-neighbor coordination with distances d from 2.32 to 2.37 Å and bond angles slightly above 100°. This is a familiar consequence of the $4s^24p^4$ valence electronic structure. All crystalline forms have intermolecular distances significantly smaller than the van der Waals distance[6] (4 Å) and intermolecular bonds play an important role in determining the electronic and geometric structures and the properties of the various Se forms.[2–4,7] This distinguishes polymeric Se allotropes from polymers with weakly interacting chains, such as polyethylene. The existence of three high-pressure phases of crystalline Se between 14 and 50 GPa has recently been established.[8] The application of pressure leads to increased interchain interactions in t-Se with transitions to threefold, fourfold, and finally sixfold coordinated monoclinic, tetragonal, and rhombohedral phases.

Second, selenium readily forms glasses, and its elemental nature and accessible glass transition temperature (T_g ~310 K) make it a prototype of such systems. Using topological arguments, Phillips[9] showed that covalent materials with an average coordination number $\langle N\rangle \leq 2.4$ are potential glass formers, i.e., they yield amorphous structures when quenched from the melt at modest rates. Amorphous Se, with $\langle N\rangle$ ~2.0, is "underconstrained" and retains a significant amount of configurational freedom even with fixed bond lengths and angles. This is reflected in the distribution of dihedral angles (the angle between the planes defined by the first and second trimers in a four-member chain) and longer-range correlations, and is the origin of the intermediate-range order observed.[10] The polymerization in the solid phase from either Se_6 or Se_8 molecules to Se_∞ chains is directly observable via differential scanning calorimetry (DSC),[11] in contrast to sulfur, where polymerization proceeds in the liquid phase.[12]

Third, and most important, the photoconducting and semiconducting properties of selenium—particularly its amorphous form—have led to important applications, such as photocopying machines and rectifiers. The photoconductivity and photodarkening phenomena are thought to be linked to the nature and concentration of the "defects" in this material,[13–17], i.e., the deviations from optimal twofold coordination in t-Se and the ring molecules. Laser-induced vitrifaction and crystallization of Se and Se alloys show promise of becoming viable processes for storing data on rewritable optical disks.

It is not surprising that much experimental information has accumulated on the disordered phases of

TABLE I. First- and next-nearest-neighbor distances d and d_{NN} (in Å), and bond angles α for α-monoclinic (Se_8), rhombohedral (Se_6), trigonal (Se_∞), "free" Se chains in mordenite (M-Se), amorphous selenium (a-Se), and liquid selenium (ℓ-Se). The number of atoms in the neighbor shells is given in parentheses, subscripts e and i denote intermolecular and intramolecular distances, respectively.

	α-Se_8[a]	Se_6[b]	Se_∞[a]	M-Se[c]	a-Se[d]	ℓ-Se[e]
d	2.34_i (2)	2.36_i (2)	2.37_i (2)	2.33_i (2)	2.32-2.36_i (1.9–2.3)	2.34
α	106°	101°	103°	102°	105°	
d_{NN}	3.48_e (4)	3.41_e (2)	3.44_e (4)	3.61_i (2)	3.6-3.8_{i+e} ($\sim 6-7$)	
	3.71_i (2)	3.47_e (1)	3.68_i (2)			
		3.64_i (2)				

[a] Reference 4.
[b] Reference 11.
[c] Reference 22.
[d] Reflecting the range of numbers given in the experimental work referenced in this article.
[e] Reference 33.

Se:[18] X-ray and ultraviolet photoemission spectroscopy (XPS,UPS),[19,20] optical and vibrational spectroscopy,[10,12,21–24] nuclear magnetic and electron spin resonance,[25] Mössbauer spectroscopy,[26] mechanical properties and viscosities,[27] calorimetric and other types of thermodynamical data,[28] transmission electron microscopy,[29] and numerous neutron and x-ray scattering data including extended x-ray-absorption fine structure.[30–41] In spite of the wealth of experimental information, however, the underlying atomic structures of amorphous and liquid Se remain controversial, due, in part, to the sensitivity of many measurable properties to preparation conditions, thermal history, and impurity content (e.g., oxygen) of the samples. Therefore, "amorphous selenium" is not a material with a unique structure, and similar ambiguities may be expected in different samples of liquid Se.

Many structural models have been proposed. They often conflict, even if apparently supported by more than one experiment. On the basis of early x-ray and neutron-scattering data, Henninger *et al.*[30] concluded that a-Se consisted of Se chains in random orientation and "liquidlike atomic assemblage." Kaplow *et al.*[31] were led by their x-ray data to conclude that a-Se is a molecular solid made up of distorted Se_8 molecules. Richter[32] pictured the constituents as planar zig-zag chains, joined to layers. Robertson[20] and Lucovsky and Wong[10,12] were among the first to note that radial distribution functions from scattering experiments alone are insufficient to distinguish between the various models.

The source of difficulty can be seen in Table I, which shows that both the first and next-nearest-neighbor distances are very similar in all crystalline Se modifications. Models based solely on the small differences between these forms cannot be expected to explain all the measured features, particularly in view of the sensitivity of the latter to the preparation conditions. However, the table does display a clear trend concerning the relative strengths of intramolecular and intermolecular bonds. As is well known from confining single Se helices in linear mordenite channels,[22,34] a reduced intermolecular coupling leads to increased intramolecular bonding and shorter nearest-neighbor distances. Table I shows that the short-range order in a-Se resembles more that of "free" chains, with weaker interchain interactions than in t-Se, possibly due to misalignment of chains or rings, or both.

Robertson[20] and Lucovsky and Wong[10,12] developed a static model for the structure of a-Se based on additional information from XPS/UPS and infrared (ir) spectra and comparison with parametrized calculations for the electronic density of states (DOS) and the ir response. In this popular model, the vast majority of atoms are in chains—with bond distances and bond angles narrowly distributed about the t-Se and Se_8 values—and the monomer content is low ($< 5\%$). The intermediate range order consists of a narrow distribution of the dihedral angle γ about the energetically most favorable[42] value of $\sim 100°$. In most crystalline forms γ is near 100°, but it varies widely with a characteristic pattern in some small Se_n molecules.[43] Note that the phase of dihedral angles in any five-atom fragment determines whether the configuration is helixlike ("*trans*," ++ or − −) or ringlike ("*cis*," + − or − +). The model of Robertson,[20] Lucovsky and Wong[10,12] is a pattern of randomly varying signs of the (fixed) dihedral angle along extended chains. Extreme examples of this "motif" are helical Se_∞ (++++++ ⋯ or − − − − − − ⋯) or Se_8 rings (+ − + − + − + −). Amorphous Se could then contain five- or six-atom fragments of rings within the chains and show fingerprints of rings in the ir spectrum.[12] Interpretations[44] of early CS_2 dissolution experiments indicating a significant Se_8 fraction[45] were shown to be unreliable due to uncontrolled illumination conditions[12] and rapid, concentration-dependent equilibration reactions[46]

$$Se_\infty \rightleftharpoons Se_8 \rightleftharpoons Se_7 \rightleftharpoons Se_6. \quad (1)$$

Misawa and Suzuki[47] proposed a similar disordered chain model for liquid selenium, and computed ring and chain fractions as functions of temperature from the same erroneous data.[45] Their fitted energy difference between

cis− (++) and *trans*− (+ −) sequences (27 meV/atom) is probably an overestimate, and the question of the relative role of rings versus chains in ℓ- and a-Se is still unsettled. Structural aspects of ℓ-Se, in particular, have received recent attention in experimental work on a semiconductor-metal transition. Tamura[48] investigated thermodynamical, electronic, and structural properties near the liquid-gas critical point. On the basis of optical absorption and x-ray-diffraction measurements it was concluded that approximate twofold coordination persists into the metallic range up to 1500 °C and 510 bars, with an average chain length of only about seven atoms reducing the coordination number slightly below $N_1 \sim 2$. This is consistent with other experimental work,[49] where a markedly different short-range order with $N_1 \sim 3$ was reported only at much higher pressures ($\geq$ 80 000 bars). The coordination in the semiconducting liquid phase investigated in the present work therefore appears representative up to relatively high pressures.

Although a detailed molecular-dynamics (MD) study would offer a direct view into the microscopic structure and could shed light on a number of these issues, we are unaware of any such investigation to date. Long *et al.*[50] used simple empirical two-, three- and four-body forces acting on a small number of initial structures to obtain radial distribution functions, structure factors, and dihedral angle distributions for comparison with scattering experiments. A much more detailed MD study employing state-of-the-art empirical interatomic potentials has been carried out for sulfur by Stillinger *et al.*[51] The main aims of these authors, however, were special aspects of the static structure and not dynamic properties. They also pointed out the limitations of even carefully constructed empirical few-body potentials in highly anisotropic covalent systems such as group-VIA elements.

We present here what we believe to be the most realistic MD simulation of ℓ- and a-Se performed to date. The interactions between 64 Se atoms in a constant volume simple cubic (SC) cell were computed with a quantum-mechanical method described in Sec. II, avoiding the difficulties with empirical, truncated potentials. Sec. III A gives our results for a-Se and ℓ-Se and discusses the short- and intermediate-range order in conjunction with experimental data where available. In Sec. III B this information is used to compare with previous models for a-Se, and we present an extended model. Sec. III C is devoted to structure and stability of the defects and our concluding remarks follow in Sec. IV. A preliminary report has been presented elsewhere.[52]

II. METHOD OF CALCULATION

A. Formalism

The method we use has been described in detail previously.[53,54] It combines the density-functional (DF) formalism[55] and molecular dynamics, and avoids the parametrization of interatomic forces common in MD simulations. We have demonstrated the applicability of MD-DF to structural and dynamical properties of group VA and VIA elements in a variety of cluster studies.[43,54,56–60] In the MD-DF formulation, the electronic wave functions $\{\psi_i\}$ are treated as dynamical variables and a corresponding kinetic-energy term appears in the Lagrangian

$$\begin{aligned}\mathcal{L} = &\sum_i \mu_i \int_\Omega d\mathbf{r}\ |\dot{\psi}_i^* \dot{\psi}_i| \\ &+ \sum_{i,j} \Lambda_{ij} \left(\int_\Omega d\mathbf{r}\ \psi_i \psi_j^* - \delta_{ij} \right) \\ &+ \sum_I \frac{1}{2} M_I \dot{\mathbf{R}}_I^{\,2} - E[\{\psi_i\}, \{\mathbf{R}_I\}] \end{aligned} \tag{2}$$

(first term). Here M_I and $\mathbf{R}_I$ denote the ionic masses and coordinates, μ_i are fictitious "masses" associated with the electronic degrees of freedom, dots denote time derivatives, and the Lagrangian multipliers Λ_{ij} are introduced to satisfy the orthonormality constraints (second term) on the $\psi_i(\mathbf{r},t)$. For the potential energy surface for the ions $E[\{\psi_i\},\{\mathbf{R}_I\}]$ we use the Kohn-Sham functional

$$\begin{aligned} E[\{\psi_i\},\{\mathbf{R}_I\}] = &\sum_i \langle \psi_i(\mathbf{r}) | -\frac{\nabla^2}{2} | \psi_i(\mathbf{r}) \rangle \\ &+ \int d\mathbf{r}\, n(\mathbf{r}) \left(V_{\rm ext}(\mathbf{r}) + \frac{1}{2}\Phi(\mathbf{r}) \right) \\ &+ E_{\rm xc}[n(\mathbf{r})] + \frac{1}{2} \sum_{I \neq J} \frac{Z_I Z_J}{|\mathbf{R}_I - \mathbf{R}_J|} . \end{aligned} \tag{3}$$

$\Phi(\mathbf{r})$ is the Coulomb potential, $E_{\rm xc}$ the exchange-correlation energy, and $V_{\rm ext}$ the field of the ions. For $E_{\rm xc}$ we adopt the widely used local-density (LD) approximation,

$$E_{\rm xc}^{\rm LD} = \int d\mathbf{r}\ n(\mathbf{r})\ \varepsilon_{\rm xc}[n(\mathbf{r})], \tag{4}$$

where $\varepsilon_{\rm xc}[n]$ is the exchange and correlation energy per particle of a homogeneous electron gas with density n. This approximation yields reliable binding energy trends (i.e. shapes of energy surfaces) and equilibrium structures for many molecules and solids.[55] We use here the electron gas parametrization of Vosko *et al.*[61] The single electron eigenstates ψ_i used to construct the density $n(\mathbf{r},t) = \sum_i |\psi_i(\mathbf{r},t)|^2$ are expanded in the plane-wave basis

$$\psi_i(\mathbf{r}) = \psi_{j\mathbf{k}}(\mathbf{r}) = \sum_{n=1}^{M} c_j^{\mathbf{k}}{}_{\mathbf{G}_n} \exp[i(\mathbf{k}+\mathbf{G}_n)\cdot\mathbf{r}], \tag{5}$$

and a local pseudopotential representation was chosen for the electron-ion interaction $V_{\rm ext}$,[62]

$$\begin{aligned} V_{\rm ext}(\mathbf{r}) &= \sum_I v_{ps}(\mathbf{r} - \mathbf{R}_I)\ , \\ v_{ps}(\mathbf{r}) &= \frac{Z}{r} \frac{1 - e^{-\lambda r}}{1 + e^{-\lambda(r - r_c)}}\ . \end{aligned} \tag{6}$$

The potential parameters r_c and λ were optimized by fitting the tails of the valence electron orbitals to those of an all-electron calculation.[43] The equations of motion derived from Eq. (2)

$$\mu\ddot{\psi}_i(\mathbf{r},t) = -\frac{\delta E}{\delta\psi^*(\mathbf{r},t)} + \sum_k \Lambda_{ik}\psi_k(\mathbf{r},t)\,, \tag{7}$$

$$M_I\ddot{\mathbf{R}}_I = -\nabla_{\mathbf{R}_I}E\,, \tag{8}$$

were solved using the Verlet algorithm. The artificial Newton's dynamics for the electronic degrees of freedom, together with the choice $\mu_i \ll M_I$, effectively prevent transfer of energy from the classical to the quantum degrees of freedom over long simulations.

B. Computational details

We represent bulk ℓ- and a-Se by 64 atoms in a SC unit cell with lattice constant $a = 12.9$ Å and periodic-boundary conditions. The resultant density $\rho = 3.91$ g cm^{-3} corresponds to liquid Se at ambient pressure and $T = 573$ K,[63] near the center of the temperature range 350–720 K of interest here. The thermal density dependence of liquid Se at 491 K has been given as -5×10^{-4} g cm^{-3}K^{-1}. Isochores show a pressure slightly higher than 1 kbar at the density and upper temperature we have chosen.[64,18] Therefore a comparison of our results with constant pressure data in this limited temperature range appears justified. The cutoff energy for the plane-wave expansion Eq. (5) was 7 a.u., leading to ~14 000 plane waves for each of the 192 occupied electronic states at a single k point in the Brillouin zone ($k = \Gamma$, the only high-symmetry point in disordered systems). The parameters in the local pseudopotential [Eq. (6)] were $r_c = 0.924$ a.u. and $\lambda = 10.4$ a.u.$^{-1}$. Cutoff energy and pseudopotential parameters were taken from previous work,[43] where they satisfied the stringent test of giving accurate energy surfaces for small selenium clusters. In that work, bond distances, bond angles, and dihedral angles for Se_6 and Se_8 agreed with experimental data to about 1%, and atomization energies were overestimated by about 1 eV/atom. A uniform overestimate of that size is common in applications of the LD approximation, but binding energy *trends*, shapes of energy surfaces, and relative depths of different minima are given reliably.[55]

With appropriate values of μ (1800 a.u.), M (~ 143 600 a.u.), and integration time step Δt (3.4×10^{-16} s), the equations of motion Eq. (8) are integrated accurately, with one time step taking about 25 s of CPU time on a Cray X-MP 416 computer.

C. MD procedure and thermal treatment

The initial configuration comprised 64 Se atoms on a slightly perturbed simple cubic lattice (Fig. 1), with six-fold coordinated atoms at nearest-neighbor distances of ~6.1 a.u. For this geometry, we determined those ψ_i that minimize E, using an efficient self-consistent iterative diagonalization technique, such as described by Štich *et al.*[65] With the electrons initially in their ground state, the dynamics [Eq. (8)] generate Born-Oppenheimer trajectories without constantly requiring additional diagonalization and self-consistency cycles for the electrons over several thousand time steps. During the microcanonical

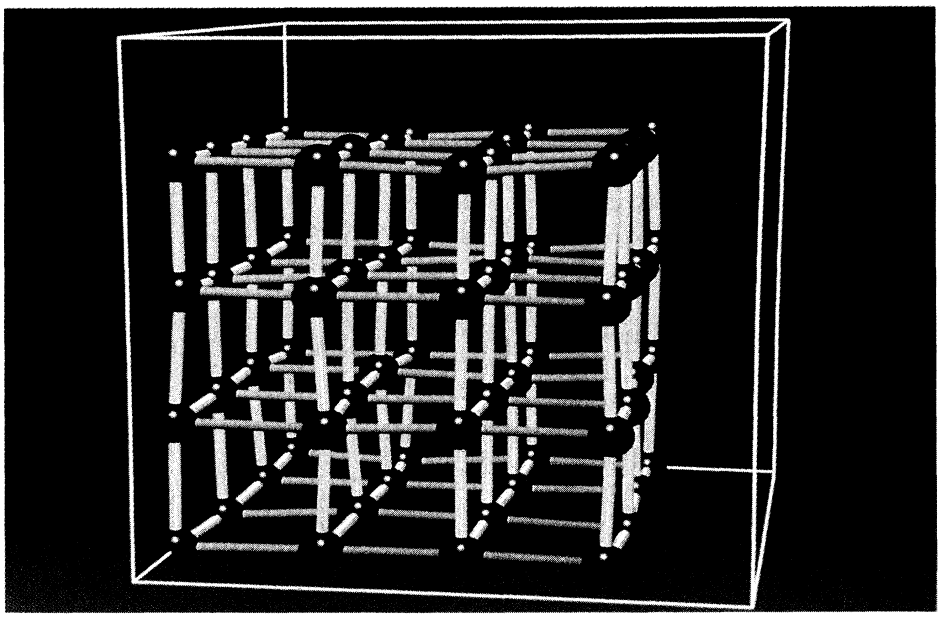

FIG. 1. Ball-and-stick model of the starting geometry used for the MD-DF simulation. 64 Se atoms were placed on randomly perturbed simple cubic lattice sites with the coordination number 6. The initial atomic spacing is ~6.1 a.u. Only atoms and bonds inside the periodically repeated cube are shown.

MD runs, the maximum deviation from the ground-state energy of the system of 384 electrons was 0.3 eV at $\langle T\rangle =$ 720 K and 0.15 eV at $\langle T\rangle =$ 350 K. To achieve this level of convergence, it was necessary to quench the electronic subsystem every few thousand time steps.

Once in the initial electronic ground state, the system was melted at $T \sim 2500$ K and the temperature then lowered in steps to 720 K, where the system was equilibrated. This initial thermal treatment took 2500 Δt (0.85 ps, approximate cooling rate 4×10^{15} K s^{-1}) and the atoms moved an average of $\sim \frac{3}{4}$ of a typical Se—Se single bond length, reaching approximate twofold coordination towards the end.

The system was then separated from the heat bath and evolved microcanonically for 13 500 steps (4.6 ps). This will be referred to subsequently as the 720 K trajectory. After 5000 of these steps, two different MD paths were pursued. The first was an annealing in steps to and equilibration at 350 K (duration 10 600 steps, 3.6 ps) followed by 13 200 steps microcanonical evolution (4.5 ps, the 350 K trajectory) for temporal averaging. The second was an instantaneous quench and equilibration at 350 K followed by a microcanonical trajectory of 3000 steps. The latter was undertaken in order to check the influence of the quench rate on our results and will be discussed below. To investigate the *local* stability of the defects, the system was quenched at the end of the 4.5 ps run at $\langle T\rangle = 350$ K into the nearest local minimum via steepest descents techniques.[65]

Relatively long MD runs are necessary to rule out artifacts caused by poor equilibration in a high viscosity, slowly diffusing system such as Se. In ℓ-Se, for example, the mean-square displacement $\langle \sum_i [\mathbf{r}_i(t) - \mathbf{r}_i(0)]^2 \rangle$ has a linear dependence on time only after 0.8 ps of the trajectory. The corresponding self-diffusion coefficient (1.10×10^{-5} $cm^2 s^{-1}$) is in good agreement with the value deduced from scattering experiments (0.95×10^{-5} $cm^2 s^{-1}$).[41] Diffusion at T=350 K was too slow to be quantified reliably.

III. RESULTS AND DISCUSSION OF THE MD SIMULATIONS

A. Short- and intermediate-range order

We now compare our computed short- and intermediate-range correlation functions with available experimental data. The data comprise two-body [pair distribution, $g(r)$], three-body [bond-angle distribution, $A(\alpha)$], four-body [dihedral angle distribution, $D(\gamma)$], and five-body correlation functions (dihedral angle phases). Much of this information is not directly accessible to experimental evaluation and will be used later to gain insight into the atomic structures of a-Se and ℓ-Se and to assess the validity of earlier models of a-Se.

1. Pair distribution functions

In Fig. 2 we compare the pair distribution functions $g(r)$ from our simulation with those obtained at almost identical temperatures in a recent high-resolution neutron-scattering study.[37] The theoretical curves have been broadened with the experimental resolution according to the procedure used by Etherington *et al.*[66] The main features agree very well for a- and ℓ-Se, with small deviations in peak intensity and position. It should be noted, however, that $g(r)$ curves derived from $S(Q)$ scattering data depend somewhat on light sources used, resolution, sample density and preparation, and details of the Fourier transform method used to obtain $g(r)$ (see Refs. 30, 31, 36, 37, and 39).

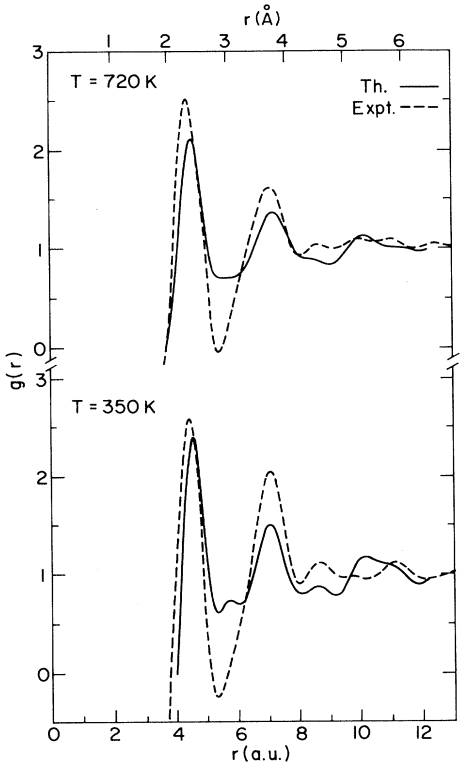

FIG. 2. Pair distribution functions $g(r)$ obtained from MD-DF simulation and experiment (Ref. 37) for liquid and amorphous selenium. The theoretical curve is broadened with the experimental resolution for proper comparison. Oscillations below the first peak in the experimental curve due to a raw Fourier transform have been omitted.

Our calculations show two prominent peaks in both disordered phases (a-Se: 2.41 and 3.73 Å ; ℓ-Se: 2.39 and 3.79 Å), but no sign of the intricate long-range correlations present in the crystalline forms.[35] A further collapse of the network structure in the liquid leads to the expected reduction in nearest-neighbor distance and to the larger second-neighbor separation mentioned above. Apart from this phenomenon and thermal broadening of peaks in the liquid, the pair distributions suggest very similar radial order in amorphous and liquid Se. These findings are reflected in the experimental curves, with some disagreement (less than ~3 %) in the peak positions. Such small discrepancies could be due to the specific pseudopotential approximation we use, to the

plane wave basis and/or the fixed density approach. We note that the a-Se trajectory following the instantaneous quench from 720 K to 350 K (see Sec. II C) shows little of the characteristic differences from the $g(r)$ diagram of ℓ-Se. With a significant "memory" of ℓ-Se, peak positions and widths are almost identical, emphasizing the need for a slower annealing to resolve differences.

The area under the first and second peaks in the (original, unbroadened) pair distribution function gives the nearest and next-nearest neighbor coordination numbers N_1 and N_2, respectively. We find that both a- and ℓ-Se have an average coordination number $N_1 = 2.1 - 2.2$ that is well within the range quoted by most experimental studies (see Table I). At both temperatures, the second-neighbor range between 5.2 and 8.0 a.u. contains on average another $N_2 \sim 7$ atoms. Table II shows the distribution of first-neighbor coordination numbers found in our MD simulations that leads to the average N_1 values mentioned above. These distributions remain practically constant along the trajectories taken, indicating that equilibration artifacts are not significant: If we average only over the last 3000 steps of each trajectory, the numbers remain unchanged for ℓ-Se but show a small tendency towards increased twofold coordination for a-Se (3%, 82%, 14%, and 2% being the concentration of onefold-, twofold-, threefold-, and fourfold coordinated atoms, respectively). The only visible difference between amorphous and liquid Se is the slightly higher proportion of singly coordinated atoms in the liquid phase, and this can be attributed to more frequent bond breakings at higher temperatures. A rough estimate for the bond breaking frequency Γ can be deduced by counting events in the MD cell that lead to bonds stretching beyond $r_{\min} = 5.2$ a.u. For ℓ-Se, we obtain $\Gamma \sim 2$ ps^{-1} (per atom), for a-Se $\Gamma \leq 1$ ps^{-1}. The vast majority of atoms is twofold coordinated as in the crystalline forms. This has been known since the first scattering experiments were performed on a-Se,[30,31,39] and recent careful experiments have shown it for the semiconducting liquid as well.[36,48]

The concentration of threefold coordinated atoms in the MD cell is $\sim 15\%$ at both temperatures, and is higher than expected from experimentally derived $g(r)$ curves.[36] Although most experiments lead to an average coordination number slightly above 2.0, a fact that can only be rationalized with a nonvanishing fraction of more highly coordinated atoms, we believe that the rapid quenching procedure we use leads to an upper bound for the number of coordination defects regardless of type. In principle, a pressure-induced increase in threefold atoms is conceivable in a constant-volume simulation, but this effect can only play a minor role here: The number of overcoordinated atoms is almost identical at T=720 and 350 K, and the (ρ, T) diagram[18] for ℓ-Se indicates only a small pressure increase. Therefore, the almost constant concentration at T=720 and 350 K over trajectories several ps long indicates that threefold coordinated atoms and chain branching contribute considerably to the properties of ℓ- and a-Se. The number of atoms with $N_1 > 3$ in our cell is small, but an average of one fourfold coordinated atom in a-Se allows us to study such defects.[13]

TABLE II. Distribution of first-neighbor coordination numbers N in the MD-DF simulations of Se at T=720 K and T=350 K. The upper integration limit, i.e., the first minimum in $g(r)$, was 5.2 a.u. in both cases (see Fig. 2). We show the temporal average percentage (over the whole length of the trajectories) of atoms with coordination number N.

N	ℓ-Se ($T = 720$ K)	a-Se ($T = 350$ K)
1	8	4
2	75	77
3	16	17
4	1	2

The phonon density of states can be computed easily by a Fourier transform of the velocity autocorrelation function, and provides further evidence that our simulation overestimates the defect concentration. We obtain good agreement with inelastic-neutron-scattering experiments for a-Se (Refs. 38 and 40) for the three main peaks representing torsion, bending and stretching modes (theor., 52, 114, and 269 cm^{-1}; expt., 44, 129, and 260 cm^{-1}, respectively[38]). However, while experiment shows a gap between $\sim$150 and 200 cm^{-1}, our calculations lead to a pronounced peak at 185 cm^{-1} that we attribute to the higher proportion of defects in our sample. Several small shoulders also appear in the torsion and bending region that are not observed in the scattering spectra of a-Se.

2. *Partial pair distribution functions*

It is illuminating to decompose $g(r)$ into contributions from atoms with different N_1. Figure 3 shows the partial pair distribution functions $g_{ij}(r)$ between i- and j-fold coordinated atoms, and the dominance of twofold contributions g_{22} is evident. Twofold coordinated atoms are bonded primarily to other twofold atoms with interatomic distances of $d_{22} = 2.39$ Å (a-Se) and $d_{22} = 2.37$ Å (ℓ-Se). Threefold coordinated atoms (see Sec. III C for more details) are mainly bonded to twofold atoms with $d_{32} = 2.47$ Å. The bonds between pairs of threefold coordinated atoms are even longer, $d_{33} = 2.65$ Å (ℓ- and a-Se). This elongation of bonds to group-VIA elements with increased coordination is known from previous theoretical work[67] (geometries of C_1 and C_3 defects) and supported by chemical evidence[13,42,58] (e.g., S—S bonds are longer and weaker in —S—SO—S— than in —S—S—S— groups). It is interesting that the opposite trend can be observed for the second-neighbor peaks in Fig. 3.

Figure 3 also helps explain the absence in the computed $g(r)$ functions (Fig. 2) of the pronounced minimum between the first and second peaks in the experimental curves. The probable overestimation of the number of threefold coordinated atoms leads to significant g_{23} and g_{33} contributions in precisely that region. The small hump in the theoretical $g(r)$ for a-Se near 3.0 Å (5.7

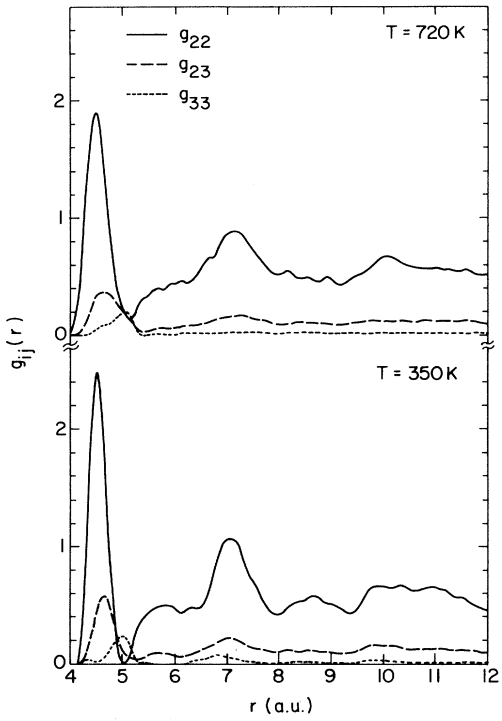

FIG. 3. Partial pair distribution functions $g_{ij}(r)$ $(i,j = 2,3)$ for ℓ- and a-Se. The first neighbor coordination shell was defined by the first minimum in $g(r)$ at 5.2 a.u. (see text). No broadening was applied.

a.u.), which can be termed intermolecular or interchain distance correlations between twofold coordinated atoms (see g_{22} in Fig. 3), is obscured by thermal vibrations and by the presence of the threefold atoms at T=720 K. Its appearance is independent of the quenching rate, i.e., the position and shape are identical in the a-Se trajectory following an instantaneous quench from 720 K to 350 K (see Sec. II C) and are unlikely to be an artefact of the fast cooling procedure required by MD-DF. A similar feature has been observed in several scattering studies,[35,36,39] but it lies in a region most sensitive to experimental resolution and the method used to obtain $g(r)$ from $S(Q)$ and could not be identified unambiguously.

3. Static structure factor

The static structure factor $S(Q)$ provides a further set of experimental data for assessing the accuracy of our MD simulation. Figure 4 compares the $S(Q)$ obtained by Fourier transforming $g(r)$ with the experimental function for a-Se over the complete Q-range investigated.[37] Apart from the first sharp diffraction peak (FSDP), the agreement of peak locations and intensities is excellent, and even the oscillation between third and fourth peak in the experimental curve is evident. A uniform broadening of the theoretical curves is to be expected because of the finite radial cutoff used in the Fourier-transform procedure. It is difficult to link the origin of the deviation in the position of the FSDP (theory, 1.35 a.u.$^{-1}$; experiment, 1.01 a.u.$^{-1}$) to a particular deficiency in the theoretical $g(r)$ function, because of the nonlocal Fourier transform used to obtain one from the other. However, the shape and position of the FSDP should be affected most by real-space features near $r = 2\pi/Q \sim 6.3$ (expt.) and 4.7 a.u. (theor.), corresponding to the region near the first minimum and second maximum in $g(r)$. We found that the FSDP is indeed most sensitive to changes in shape, intensity, and position of the second-neighbor peak in $g(r)$, where the agreement with the experimental pair correlation function is not perfect. Test calculations indicate that neither the long-range behavior of $g(r)$ near the edge of the MD cell nor the concentration of threefold coordinated atoms had a noticeable impact on the position of the FSDP.

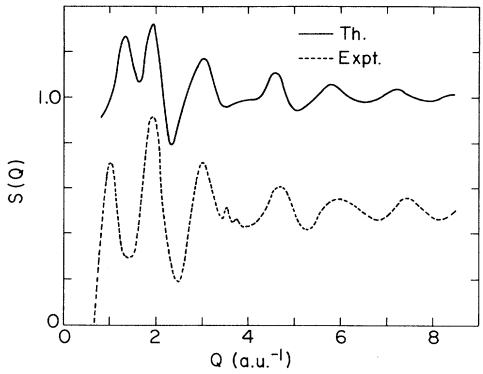

FIG. 4. Comparison of theoretical and experimental (Ref. 37) static structure factors $S(Q)$ for a-Se in comparison. The experimental curve has been shifted by −0.5.

Figure 5 shows the $S(Q)$ functions in more detail in a range where both ℓ- and a-Se experiments have been published.[37] The agreement between theoretical and experimental $S(Q)$ diagrams is equally good for liquid and amorphous Se. Moreover, all significant differences between the ℓ- and a-Se structure factors are reproduced well in the theoretical curves (see Fig. 5). Upon raising the temperature, (a) all four peaks shown undergo a small shift to lower Q, (b) the intensity of the first peak is reduced dramatically, and (c) all peaks are broadened.

The comparison of computed $g(r)$ and $S(Q)$ functions with experimental data shows that our simulation gives an accurate picture of the local order and distance correlations in ℓ- and a-Se. As noted in Sec. I, two-body correlations are an insufficient basis for a microscopic model of these substances. We now discuss three-, four- and five-body correlation functions that are not directly accessible to experiments, although some circumstantial evidence from scattering and spectroscopy data does exist.

4. Bond-angle distribution

The first and second peaks in pair distribution functions derived from scattering experiments can be ex-

ploited to give a highly averaged value of $\sim$ 105° for the bond angle in amorphous Se.[22,34,35] The bond-angle distribution functions $A(\alpha)$ shown separately for twofold- and threefold coordinated atoms in Fig. 6 are consistent with this value but reveal more information. $A_2(\alpha)$ is singly peaked and centered symmetrically at $\alpha = 103°$. The only visible temperature effect is a small thermal broadening (standard deviations of the data points 10° and 13°, full width at half maximum values of 21° and 26° at 350 and 720 K, respectively). The similarity between liquid and amorphous phases is also reflected in the negligible effect of the quenching rate on the bond-angle distribution function. The annealed and instantly quenched a-Se trajectories (see Sec. II C) are practically identical in this respect.

Inspection of Table I shows that the center of the distribution lies close to the bond angles of all crystalline Se modifications and is practically identical to the value found in the Se helices of t-Se and M-Se. Values in that range were found to be energetically the most favorable in Se and S clusters with up to 13 atoms in our previous work.[43,54] Angles larger than 110° or smaller than 100° occurred only in the smallest clusters $(S,Se)_{3-5}$ with significant ring strain.

The relatively large number of threefold coordinated atoms in our MD cell allows us to derive with accurate statistics a separate bond-angle distribution function (see Fig. 6). A trimodal distribution with maxima around 90°, 110°, and 180° indicates the possible existence of several geometrically different threefold defect types in amorphous Se (see Sec. III C). $A_3(\alpha)$ is spread out more than A_2 and the only apparent effect of a temperature increase is again a thermal broadening (standard deviations 26° and 28° at 350 and 720 K, respectively).

5. Dihedral angle distribution

The crucial role played by the dihedral angle γ and its variation in the structural chemistry of twofold coordinated sulfur and selenium allotropes and compounds is well known.[5,13,42] The bond distance and bond-angle potential functions are steeper than the dihedral angle potential, so that γ can be distorted more easily than any other molecular parameter. In a simplified molecular orbital picture, the p "lone-pair repulsion" on adjacent atoms is responsible for (a) the energetically optimal value of near 90° for an isolated chain of four Se or S atoms and (b) a strong coupling between the dihedral angle and the strength and length of the central bond.[54] A more thorough analysis of the orbitals involved was presented in previous LD work,[68] where the high flexibility and ease for distorting dihedral angles of single Se chains was also demonstrated. A value of γ close to 100° is the most common in all allotropes of sulfur and selenium, but large distortions from 90° occur in stable forms such as $(S,Se)_7$ crystals.[5,42,54] Apart from the marked elongation of bonds associated with dihedral angles far from 90° and minor distortions of bond angles, essentially all allotropes of S,Se, including the various rings and the polymeric chains, differ only in their pattern of dihedral angles ("motif").

For amorphous selenium, there is indirect experimental evidence that γ is distributed "over a wide range."[13,24,35,69] Raman spectra[24,46] of a-Se were interpreted in favor of chainlike molecules with dihedral angles distributed within a certain range. Andonov,[35] assuming

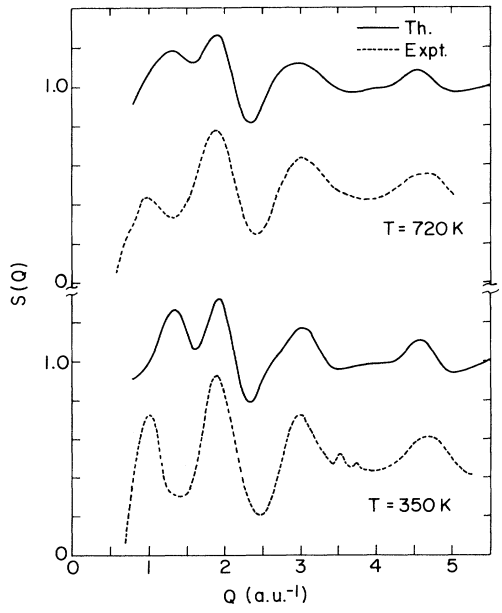

FIG. 5. Theoretical and experimental structure factors $S(Q)$ for a-Se and ℓ-Se in a smaller Q range. The experimental curves have been shifted by -0.5.

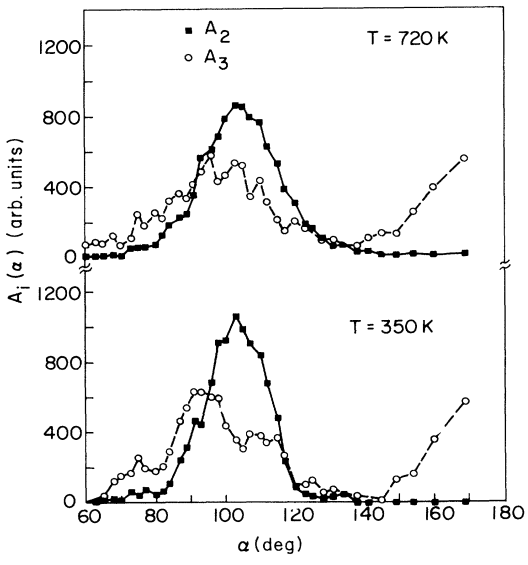

FIG. 6. Bond-angle distribution functions A_i ($i \equiv 2, 3$) for i-fold coordinated atoms in a-Se and ℓ-Se. The first-neighbor shell used to determine the coordination number has a radius of 5.2 a.u. A_2 and A_3 are normalized to the same arbitrary number.

distorted interacting chains as basic constituents, derived $74° \leq \gamma \leq 112°$ from the third-neighbor distributions obtained from x-ray data. Corb *et al.*[69] found that a simulated model (twofold coordination with bond length, bond-angle, and dihedral angle distribution as adjustable parameters), when fit to experimental radial distribution functions, gave greater agreement with a broad scatter of γ values. Long *et al.*[50] and Bellissent[37] went farther, noting that experimental $g(r)$ functions could be reproduced adequately with atomic models with a random distribution of dihedral angles.

On the other hand, Robertson[20] and subsequently Lucovsky *et al.*[10,12] proposed a "narrow" distribution of the dihedral angles in a-Se based on tight-binding calculations for ring and chainlike strings of Se atoms. The energy as a function of γ was assumed (without explicit calculations) to rise rapidly from the crystalline value, with a torsional barrier of 0.4 eV/atom. Although this is substantially greater than the experimental value for homocyclic sulfur rings (0.15–0.2 eV/atom),[13] reasonable agreement could be obtained with XPS-UPS (Ref. 20) and infrared spectra[10,12] of a-Se using a model based on *fixed* values of bond length, bond angle, *and* dihedral angle. Supplemented by a random variation of the sign of γ along chains (no closed rings), this remains a popular model for a-Se.

Figure 7 confirms that dihedral angle distortions are much more prominent in a-Se (and ℓ-Se) than both bond-angle and bond-length variations. The data support the hypothesis of Steudel[13] that γ can assume all values from 0° to 180°, with 90° being the most frequent value. A prominent maximum at $|\gamma| \sim 90°$, consistent with all experimental evidence gathered so far, is clearly visible. Apart from larger statistical fluctuations due to a much constrained thermal motion ("freezing out" of dihedral angle defects), the data at T=350 K show a maximum at $\gamma = 0°$ that is absent at T=720 K. This can be attributed to an increase in the number of planar four atom fragments with *cis* configuration in the disordered Se chains observed as main constituents (see Sec. III B). Although a precise number is difficult to give in a small system, we estimate that the temporal and number average of dihedral angles $|\gamma| \leq 10°$ is about 5% at T=350 K. We add that the annealing from 720 K to 350 K is essential to develop this feature: The instant quench trajectory (see Sec. II C) shows no indication of that second maximum.

The existence of a second maximum in $D(\gamma)$ near 0° at low temperatures is consistent with earlier LD calculations for energy hypersurfaces (T=0) of single S and Se chains.[68] It was found there that a planar zig-zag chain geometry represents a shallow local minimum and saddle point in S_∞ and Se_∞, respectively, energetically close to the ground state. Unfortunately, these authors did not consider *cis* chains with $\gamma = 0°$ and it would be very interesting to compute relative energies of isolated *trans* and *cis* chains with a traditional total-energy LDA method. On the basis of tight-binding calculations, Wong *et al.*[16] concluded that dihedral angle distortions with $\gamma \sim 0°$ or $\gamma \sim 180°$ are the intrinsic defects responsible for shallow trapping of holes and electrons in a-Se. Finally, Carroll and Lannin[24] noted the remarkable fact that the Raman peak at 250 cm^{-1} due to Se-Se stretching vibrations broadens with decreasing deposition and measurement temperature of the a-Se film used. This indicates that $D(\gamma)$ is temperature dependent, and our MD simulations support this. The broadening of the $\nu_{Se\text{-}Se}$ peak can be explained on the basis of the dependence of bond distance, bond strength, and force constant on the dihedral angle associated with the bond.[42,54] A growing proportion of dihedral angles near zero at lower temperatures will lead to an increase in the number of long, weak bonds, and the corresponding peak in the Raman spectrum broadens. A similar argument has been used with success to study structures of small S and Se clusters when single crystals were not available.[70]

Averaging over all five-atom fragments in the MD cell with no bond longer than 5.2 a.u., we find that the numbers of "ringlike" (dihedral angle phase + − or − +) and "chainlike" (++ or − −) sequences are equal to within ±5%. This agrees with the random variation in the signs of the dihedral angles in a-Se suggested by Lucovsky and Wong,[10,12] but is inconsistent with a significant energy advantage for the ring-like fragments (0.03 eV/atom) deduced from equilibration experiments.[47] However, the

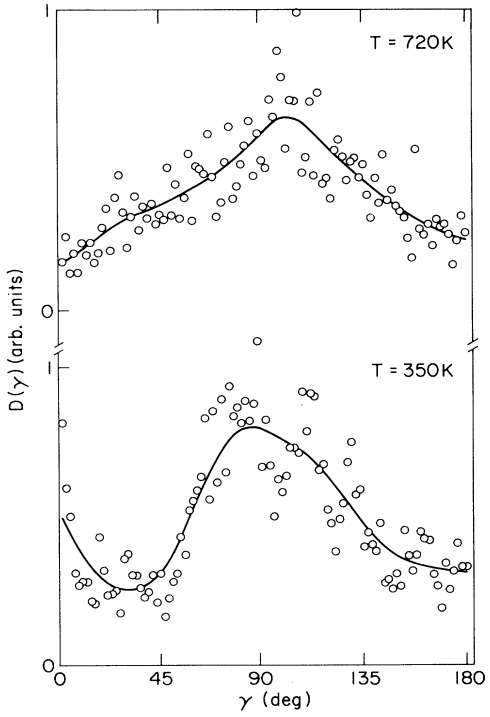

FIG. 7. Computed dihedral angle distribution $D(\gamma)$ for a-Se and ℓ-Se. $D(\gamma)$ represents the temporal and cell average for the absolute values of dihedral angles in strings of four atoms with bonds up to 5.2 a.u. The histograms (redundant data points are omitted) are normalized to the same arbitrary number and the lines provided as a guide to the eye.

analysis of these experiments assumed fixed bond distances, bond angles, and dihedral angles, while we have shown that γ, in particular, varies much more widely than often assumed.

B. Microscopic models

We can now assess the validity of models proposed previously for the disordered phases of Se and outline a new microscopic picture based on our calculations. For this purpose, we provide two "snapshots" typical of configurations in our MD simulations at T=350 K and T=720 K in Figs. 8 and 9, respectively. We show that aspects of several models can be combined into a single picture.

The early model of Henninger *et al.*,[30] though somewhat imprecise and based in part on experimental data that have not been confirmed, describes the essential ordering phenomena in a-Se remarkably well. In this model, amorphous selenium contains chain molecules like t-Se, but randomly oriented. Significant reduction in interchain correlations and rotations and stretching of the intrachain bonds are required to smear out regularities beyond second neighbors. The primary constituents of both a-Se and ℓ-Se in our calculations are chainlike molecules with up to ~20 atoms, not disordered isolated rings as suggested by Kaplow *et al.*[31] The MD cell is too small to allow us to comment on the average chain length (believed to be $10^4 - 10^5$ at the melting point) or to detect small portions of isolated rings in a bath of chains. Furthermore, the quenching rates are higher than currently attainable experimentally. Nevertheless, it is generally agreed that vibration spectra[24,10,12] and solution-extraction experiments[12,46] virtually exclude an atomic ring fraction of more than $\sim 5\%$, in accordance with our calculations. Previous investigators appear to have favored rings as primary constituents by the "more molecular" character of a-Se compared with t-Se, by its reduced interchain correlations, and also by the presence of fingerprints for rings in the vibration spectra. As discussed above, neither aspect is inconsistent with a disordered chain model.

Although we rarely observe "isolated" closed rings (i.e., where bonds with $d \leq 5.2$ a.u. are all intramolecular), this does not rule out closed paths through the *branched* network of doubly and triply coordinated *Se* atoms. Analyzing the network structure further (see Figs. 8 and 9), we can determine the size distribution of rings that form (and disappear) in the course of the simulation. At T=720 K, closed pathways through the network of Se atoms lead to variety of ring sizes, notably five, six, seven, and nine atom rings, the last occurring approximately twice as often as each of the others. This variety is reduced at T=350 K, with ring sizes increasing to 6-, 9-, and 11-membered closed paths in an approximate ratio 5:1.5:1. Because of the small unit cell, accurate ring statistics are not obtainable.

Richter[32] analyzed the the pair distribution functions in various preparations of a-Se and proposed two models—a-Se(I) and a-Se(II)—containing planar zig-zag chains ($\gamma = 180°$) with slightly different packings. Shortened zig-zag chains were also proposed as main constituents of semiconducting ℓ-Se. These models are inconsistent with our dihedral angle distribution (Fig. 7), and the incorrect conclusions resulted because interchain-intermolecular distances were mistaken for intramolecular separations.[32]

Our results support three aspects of the model of Robertson[20] and Lucovsky and Wong[10,12] for a-Se: Narrow distributions of (a) nearest-neighbor distances and (b) bond angles, and (c) a random variation of the dihedral angle phases along the primary constituents, meandering chains of Se atoms. As can be seen in Figs. 8 and 9, this can lead to ringlike fragments in the chains. We do not find the "narrow" distribution of dihedral angles that is part of their model, and we note that $D(\gamma)$ is the only quantity discussed so far that changes noticeably with temperature. Because of the link between dihedral angles and bond strength (and by that token electronic structure), empirical interatomic potentials and simple models for disordered Se cannot be expected to incorporate the essential dihedral angle behavior reliably.

It is evident that a realistic picture for a- and ℓ-Se embracing all the above aspects cannot be provided by any simple model. One important aspect concerns the behavior of ℓ-Se as "dynamical" (as opposed to purely Rouse-like) polymer with frequently breaking and reforming bonds. Faivre and Gardissat[27] pointed out that their measurements of the viscoelastic properties of Se can be explained with a combination of Rouse-like and dynamical behavior. Another aspect not included in any of the models developed to date is the role played by defects in the disordered phases of Se. Although our fast quench rate will probably lead to an overestimate of the (coordination and dihedral angle) defect concentration, a reasonable description of the microscopic picture emerging from our calculations would be "branched chains of Se atoms with bond distances and angles close to the crystalline values, and widely varying dihedral angles of random phase" (see Figs. 8 and 9).

C. Coordination defects in amorphous selenium

The approach to the structure and stability of defects in a-Se taken here is distinctly different from other methods commonly employed for that purpose (see, e.g., Ref. 67). Rather than selecting a limited number of defect geometries, computing their energies and—in some cases—relaxing the geometry locally to find the minimum in the energy surface, we analyze the network structure generated by the MD simulation at T=350 K for defect types and geometries. We then quench one configuration to its closest minimum in $E[\{\mathbf{R}_I\}]$ to investigate the local stability of the different coordination defect types and to remove bonding ambiguities. This approach avoids the arbitrary selection of defect geometries, but cannot yield information about defects that are too low in concentration to occur in the small MD cell or others that might require a specific annealing procedure.

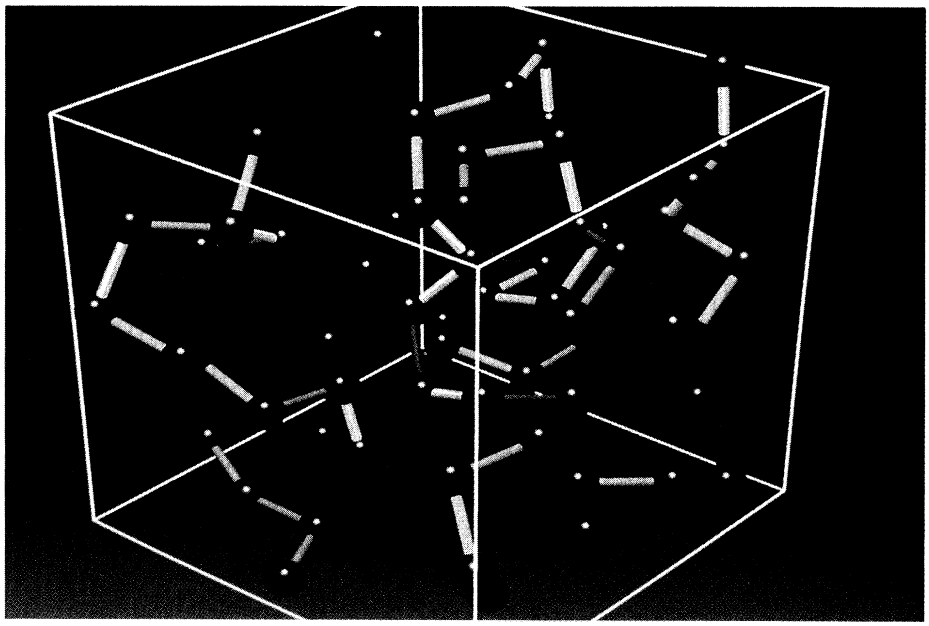

FIG. 8. Ball-and-stick model of a typical spatial configuration in amorphous selenium. All atoms inside the periodically repeated cube are shown and bonds are drawn between atoms within the cell with separation $d \leq 5.2$ a.u. Threefold coordinated atoms are shown in purple, all others in blue. Bonds to atoms in neighboring cells are omitted, so that the number of sticks is not necessarily a measure of the coordination number.

Among the numerous defect studies in a-Se, the models developed by Street and Mott,[71] Kastner *et al.*[72] and Vanderbilt and Joannopoulos[67] have received considerable attention. To explain the presence of localized states in the band gap, Street and Mott[71] proposed that dangling bonds D^0 generated naturally by breaking bonds homolytically can lead to charged centers:

$$2D^0 \rightarrow D^+ + D^- \tag{9}$$

(the symbol D denotes a defect without reference to a particular geometry or coordination). It was assumed that this reaction is exothermic by means of a substantial

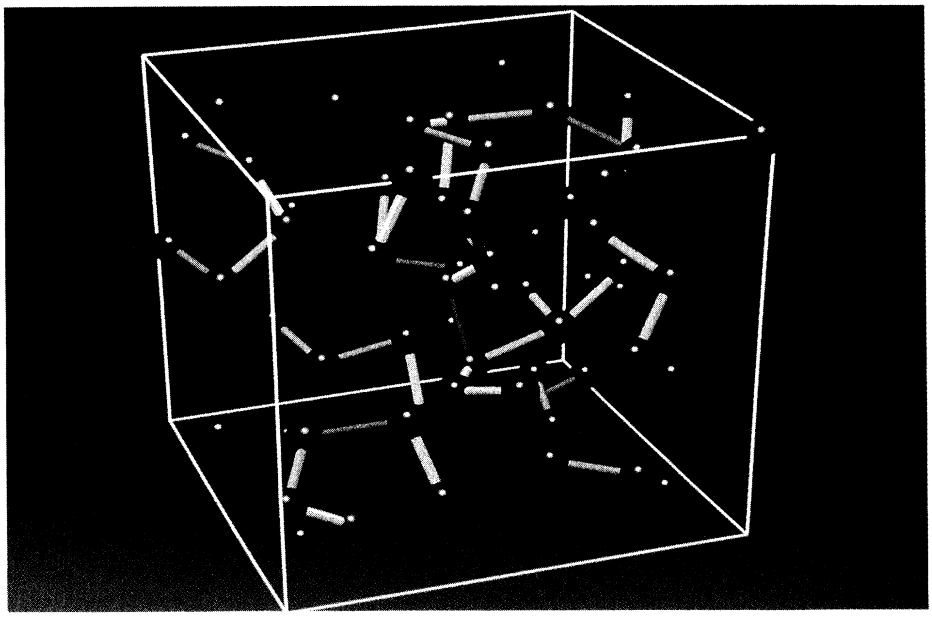

FIG. 9. Ball-and-stick model of a typical spatial configuration in liquid selenium. Threefold coordinated atoms cluster and are not as evenly distributed as in Fig. 8.

phonon contribution. Kastner *et al.*[72] attempted to analyze the possible coordination environment and electronic structure of these defects. From the exothermic nature of reaction (9), they concluded that all defects generated by homolytic bond scission will eventually become pairs of threefold coordinated cations C_3^+ and singly coordinated anions C_1^- ("valence alternation pairs", VAP's) (C denotes a chalcogen atom, and subscripts and superscripts represent coordination number and charge state, respectively). Most of the C_3^+ and C_1^- were thought to be bound together to form "intimate" VAP's (IVAP's):

$$2C_2^0 \rightarrow C_3^+ + C_1^- \rightarrow (C^+ - C^-). \tag{10}$$

However, from self-consistent total-energy LDA supercell calculations employing geometry optimization, Vanderbilt and Joannopoulos[67] showed that reaction (9) is probably endothermic. As a result, VAP's will not be the dominant defect type in a-Se, in spite of a substantial stabilizing phonon contribution. They calculated the optimal geometries for three coordination defect types, C_1^-, C_1^0, and C_3^+ and found that C_3^0 and C_1^+ relax without barrier to C_1^0 and C_3^+, respectively, when charges are constrained. Using this information, Steudel[13] proposed that hypervalent defects C_3^d-C_1^d and C_4^0 are the most frequent types (the superscripts d denote a double bonded pair).

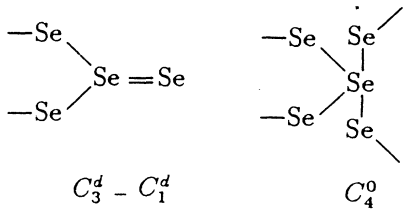

"Hypervalency"—or the presence of more than eight electrons in the chalcogen valence shell—occurs in several well-known, stable sulfur and selenium compounds (e.g., SeF_4 and SeF_6), and C_4^0 configurations are plausible reaction intermediates in reaction (1). Simple electron-pair counting arguments suggest a pyramidal geometry for C_3^d and a pseudo trigonal-bipyramidal geometry for C_4^d (with one lone pair occupying an equatorial position).

The average defect concentrations shown in Table II for a-Se do not support the assertions of Kastner *et al.*[72] and Steudel.[13] VAP's, IVAP's, and hypervalent defects of the C_3^d-C_1^d type as dominant defects would require approximately equal numbers of onefold and threefold coordinated atoms. However, our MD simulations show roughly four times as many threefold sites as onefold sites. Furthermore, we rarely observe the C_3-C_1 pairing required by the defect models of Steudel (C_3^d-C_1^d) and Kastner *et al.* (C_3^+-C_1^-, IVAP).

The defect types occurring in our a-Se and ℓ-Se MD runs are shown qualitatively in Fig. 10. They comprise C_3-C_3 and C_3-C_1 pairs, isolated C_3 and C_1 defects bonded to only twofold coordinated atoms, and a fourfold C_4 defect with a geometry close to the one proposed by Steudel.[13] In ℓ-Se, the C_3 defects show a pronounced tendency to cluster, with 82% of all threefold atoms occurring in the form of C_3-C_3 pairs, 12% as C_3-C_1 pairs, and the remainder as isolated C_3 centers. The ratio $G_{32} = \int^{r_{\min}} g_{33} / \int^{r_{\min}} g_{23} = 0.42$ is considerably larger in the liquid than that in an ideal gas mixture of N_3 threefold sites and N_2 twofold sites [$N_3/N_2 = 0.21$; $r_{\min}$=5.2 a.u., the location of the first minimum in $g(r)$]. G_{32} also remains practically constant over the whole ℓ-Se trajectory, making the C_3-C_3 pair the dominant defect type. This specific type of defect pair has not been proposed previously and has its origin in thermal motion bringing separate Se chains and chain fragments into such close proximity that chemical bonding can occur. A similar linear defect geometry (see below) has been proposed by Dembrovsky and Chechetkina[17] under the name "quasimolecular defect." Although an average over the complete trajectory still yields $G_{32} = 0.45$ ($N_3/N_2 = 0.22$) in a-Se, with 90% of all threefold atoms in C_3-C_3 pairs, a relaxation process that is slow on our MD time scale reduces G_{32} to 0.24 (57% of all threefold sites in C_3-C_3 pairs, 7% in C_3-C_1 pairs) in the final 3000 steps of the trajectory (with $N_3/N_2 = 0.17$). The C_3-C_3 pairs break up, suggesting that a "memory" of the defect states in

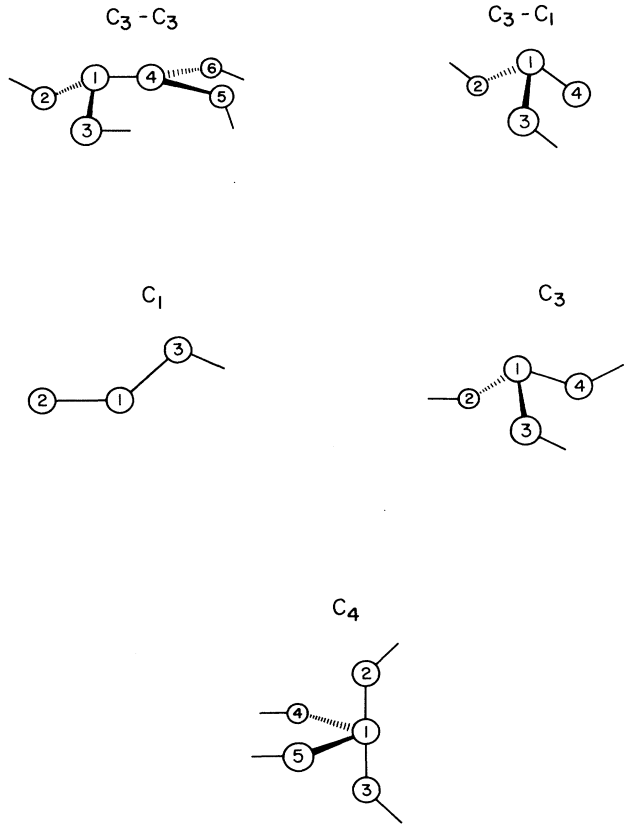

FIG. 10. Schematic drawings of the defect types encountered in the MD simulations. See Table III for geometrical parameters in the quenched a-Se sample. C denotes chalcogen atoms and subscripts the corresponding coordination numbers.

TABLE III. Geometrical parameters for the defect types encountered in the MD simulations of a-Se after quenching to T=0 (see Fig. 10 and the discussion in Sec. III C). Bond distances d_{ij} are in Å, bond angles α_{ijk} in degrees. Three different geometries (a), (b), and (c) are shown for the isolated C_3 defect.

	C_3-C_3	C_3-C_1	C_1	C_3(a)	C_3(b)	C_3(c)	C_4
d_{12}	2.30	2.38	2.36	2.75	2.49	2.51	2.49
d_{13}	2.48	2.59		2.52	2.40	2.30	2.62
d_{14}	2.61	2.31		2.47	2.47	2.66	2.49
d_{15}							2.41
d_{45}	2.42						
d_{46}	2.50						
α_{314}	105	113		118	104	90	76
α_{213}	119	71	110	164	108	98	174
α_{214}	97	109		69	74	94	98
α_{215}							75
α_{641}	174						
α_{541}	95						
α_{645}	90						
α_{415}							126

the liquid was retained in the amorphous sample due to the short time scale currently attainable with the MD-DF method. We expect isolated C_3 sites to become eventually the dominant defect type in a-Se, an assertion that is further supported by the following quench to $T = 0$.

Since the defect geometries we observe during the T=350 K MD run are subject to thermal distortions, we have quenched the system to the next local minimum in $E[\{\psi_i\}, \{\mathbf{R}_I\}]$ at the end of that trajectory, lowering the total energy E of the system by ~3.1 eV. While all the defect types discussed above are locally stable, the defect concentrations decrease significantly from their values in ℓ- and a-Se, with 3%, 9%, and 2% of the atoms onefold, threefold, and fourfold coordinated. The isolated C_3 site is the prevailing species (50% of all threefold sites) and the proportion of C_3-C_3 and C_3-C_1 pairs becomes smaller (33% and 17%, respectively, of all threefold sites). In Table III we show the geometrical parameters for the defects that are locally stable in the quenched sample. All show a lack of symmetry due to the constraints imposed by the surrounding amorphous network. The geometries of the C_3 (pyramidal) and C_1 defects are similar to those found by Vanderbilt and Joannopoulos.[67] As was suspected from the bond-angle distribution functions (see Sec. III A), two qualitatively different C_3 geometries exist: A T-shaped one with bond angles close to 90° and 180° in the C_3-C_3 pair (atoms 1, 4, 5, and 6 in Fig. 10) and pyramidal arrangements in the other cases. The C_4 defect has a geometry very close to the pseudo-trigonal-bipyramid suggested by Steudel.[13]

IV. CONCLUSIONS

We have described extensive MD simulations of amorphous and liquid selenium at 350 K and 720 K, respectively. The energy surfaces and forces are calculated using the density-functional formalism, with a local-density approximation for the exchange-correlation energy. This approach is free of the adjustable parameters common in MD calculations and has provided previously an accurate description of the structures of small Se clusters. The results for the extended systems are in close agreement with experimental data where available, and provide interesting information about the microscopic structure that is currently inaccessible to measurement. This is particularly true for the defects in the disordered systems.

The dihedral angle, one of the quantities about which little experimental information is available, plays a central role in our discussion of the structures. In our view, both amorphous and liquid selenium can be viewed as branched chains of atoms of considerable complexity, with bond lengths and angles close to the crystalline values and with widely varying dihedral angles of random phase. The importance of higher-order correlations (four- and five-body corresponding to the dihedral angle and its phase, respectively) shows the limitations to be expected from fitted potential forms, such as those that focus on two- and three-body correlations.

The fast annealing procedure required by the current implementation of MD-DF is an advantage for studying defects, since we generate significant defect numbers even in a small unit cell. Although the concentrations of the various defect types encountered are probably higher than in experiment, the computed geometries should be reliable. The present MD simulation does not support previous assertions that VAP's C_3^+-C_1^- or doubly bonded hypervalent pairs C_3^d-C_1^d are the dominant defect types in a-Se. Instead we find single threefold coordinated atoms C_3 to be the most promising candidates, leading to occasional chain branching. In the semiconducting liquid phase, the C_3 atoms form clusters.

ACKNOWLEDGMENTS

We thank R. Car, G. Galli, and M. Parrinello for many valuable discussions. We also thank D. Bock[73] and the National Center for Supercomputing Applications for expert help with the computer graphics in this article, U. Buchenau for discussions on the experimental situation, and M. Woodward for critical reading of the manuscript. The calculations were performed on the Cray X-MP 416 of the German Supercomputer Center HLRZ (Höchstleistungsrechenzentrum) in the Forschungszentrum Jülich.

---

*Present address: National Center for Supercomputing Applications, University of Illinois at Urbana-Champaign, Urbana, IL 61801.

[1] In other disordered materials the terms amorphous and vitreous generally refer to chemically prepared and substances quenched from the melt, respectively. This distinction is often not made in the case of Se and we use both terms for the same material, emphasizing either the disordered or the glassy character.

[2] *Selenium*, edited by R. A. Zingaro and W. C. Cooper (Van Nostrand Reinhold, New York, 1974).

[3] *Selenium: Gmelin Handbuch der Anorganischen Chemie, 8. Aufl., Ergänzungsband B2*, edited by H. Bitterer (Springer, Berlin, 1984); *Selenium: Gmelin Handbuch der Anorganischen Chemie, 8. Aufl., Ergänzungsband A2*, edited by H. K. Kugler (Springer, Berlin, 1980), and references therein.

[4] J. Donohue, *The Structures of the Elements* (Wiley, New York, 1974), Chap. 9.

[5] R. Steudel and E.-M. Strauss, Adv. Inorg. Chem. Radiochem. **28**, 135 (1984).

[6] L. Pauling, *The Nature of the Chemical Bond* (Cornell University Press, Ithaca, NY, 1960).

[7] R.M. Martin, G. Lucovsky, and K. Helliwell, Phys. Rev. B **13**, 1383 (1976).

[8] G. Parthasarathy and W.B. Holzapfel, Phys. Rev. B **38**, 10105 (1988).

[9] J.C. Phillips, J. Non-Cryst. Solids **34**, 153 (1979); J.C. Phillips, *ibid.* **43**, 37 (1981).

[10] G. Lucovsky and C.K. Wong, J. Non-Cryst. Solids **75**, 51 (1985); Philos. Mag. B **52**, 331 (1985).

[11] Y. Miyamoto, Jpn. J. Appl. Phys. **19**, 1813 (1980).

[12] G. Lucovsky, in *The Physics of Selenium and Tellurium*, edited by E. Gerlach and P. Grosse (Springer, New York, 1979), p. 178.

[13] R. Steudel, J. Non-Cryst. Solids **83**, 63 (1986).

[14] J. Robertson, Philos. Mag. B **51**, 183 (1985).

[15] K. Tanaka, Jpn. J. Appl. Phys. **25**, 779 (1986).

[16] C.K. Wong, G. Lucovsky, and J. Bernholc, J. Non-Cryst. Solids **97 & 98**, 1171 (1987).

[17] S.A. Dembrovsky and E.A. Chechetkina, Philos. Mag. **53**, 367 (1986); J. Non-Cryst. Solids **85**, 346 (1986).

[18] H. Endo, K. Tamura, and M. Yao, Can. J. Phys. **65**, 266 (1987).

[19] T. Takahashi, K. Ohno, and Y. Harada, Phys. Rev. B **21**, 3399 (1980).

[20] J. Robertson, Philos. Mag. **34**, 13 (1976).

[21] Y. Katayama, M. Yao, Y. Ajiro, M. Inui, and H. Endo, J. Phys. Soc. Jpn. **58**, 1811 (1989).

[22] K. Tamura, S. Hosokawa, H. Endo, S. Yamasaki, and H. Oyanagi, J. Phys. Soc. Jpn. **55**, 528 (1986).

[23] H.-P. Seyer, K. Tamura, H. Hoshino, H. Endo, and F. Hensel, Ber. Bunsenges. Phys. Chem. **90**, 587 (1986).

[24] P.J. Carroll and J.S. Lannin, Solid State Commun. **40**, 81 (1981).

[25] W.W. Warren, Jr. and R. Dupree, Phys. Rev. B **22**, 2257 (1980).

[26] C.S. Kim and P. Boolchand, Phys. Rev. B **19**, 3187 (1979).

[27] G. Faivre and J.-L. Gardissat, Macromolecules **19**, 1988 (1986).

[28] R.B. Stephens, Phys. Rev. B **30**, 5195 (1984).

[29] M. Shiojiri, Y. Hirota, T. Isshiki, K. Okashita, and S. Sekimoto, J. Electron Microsc. **12**, 281 (1989); M. Shiojiri, Y. Hirota, and T. Isshiki, *ibid.* **38**, 332 (1989).

[30] E.H. Henninger, R.C. Buschert, and L. Heaton, J. Chem. Phys. **46**, 586 (1967).

[31] R. Kaplow, T.A. Rowe, and B.L. Averbach, Phys. Rev. **168**, 1068 (1968).

[32] H. Richter, J. Non-Cryst. Solids **8**, 338 (1972).

[33] M. Inui, K. Tamura, M. Yao, H. Endo, S. Hosokawa, and H. Hoshino, J. Non-Cryst. Solids **117&118**, 112 (1990).

[34] M. Inui, M. Yao, and H. Endo, J. Phys. Soc. Jpn. **57**, 553 (1988).

[35] P. Andonov, J. Non-Cryst. Solids **47**, 297 (1982).

[36] M. Edeling and W. Freyland, Ber. Bunsenges. Phys. Chem. **85**, 1049 (1981).

[37] R. Bellissent, Nucl. Instrum. Methods **199**, 289 (1982); R. Bellissent and G. Tourand, J. Non-Cryst. Solids **35&36**, 1221 (1980).

[38] F. Gompf, J. Phys. Chem. Solids **42**, 539 (1981).

[39] F.Y. Hansen, T.S. Knudsen, and K. Carneiro, J. Chem. Phys. **62**, 1556 (1975).

[40] W.A. Phillips, U. Buchenau, N. Nücker, A.-J. Dianoux, and W. Petry, Phys. Rev. Lett. **63**, 2381 (1989).

[41] A. Axmann, W. Gissler, A. Kollmar, and T. Springer, Disc. Faraday Soc. **50**, 74 (1970).

[42] R. Steudel, Angew. Chem. **87**, 683 (1975) [Angew. Chem. Int. Edit. Engl. **14**, 655 (1975)].

[43] D. Hohl, R.O. Jones, R. Car, and M. Parrinello, Chem. Phys. Lett. **139**, 540 (1987) [Se_n clusters].

[44] A. Eisenberg and A.V. Tobolsky, J. Polymer Sci. **45**, 19 (1960).

[45] G. Brieglieb, Z. Phys. Chem. A **144**, 321 (1929).

[46] R. Steudel and E.-M. Strauss, Z. Naturforsch. Teil B **36**, 1085 (1981).

[47] M. Misawa and K. Suzuki, J. Phys. Soc. Jpn. **44**, 1612 (1978).

[48] K. Tamura, J. Non-Cryst. Solids **117&118**, 450 (1990).

[49] V.V. Brazhkin, R.N. Voloshin, and S.V. Popova, Pis'ma Zh. Eksp. Teor. Fiz. **49**, 372 (1982) [JETP Lett. **49**, 424 (1989)].

[50] M. Long, P. Gallison, R. Alben, and G.A.N. Connell, Phys.

Rev. B **13**, 1821 (1976).
[51]F.H. Stillinger, T.A. Weber, and R.A. LaViolette, J. Chem. Phys. **85**, 6460 (1986); F.H. Stillinger and T.A. Weber, J. Phys. Chem. **91**, 4899 (1987).
[52]D. Hohl and R.O. Jones, J. Non-Cryst. Solids **117&118**, 922 (1990).
[53]R. Car and M. Parrinello, Phys. Rev. Lett. **55**, 2471 (1985) (bulk Si); **60**, 204 (1988) [amorphous Si]; I. Štich, R. Car, and M. Parrinello, *ibid.* **63**, 2240 (1989) [liquid Si].
[54]D. Hohl, R.O. Jones, R. Car, and M. Parrinello, J. Chem. Phys. **89**, 6823 (1988) [S_n clusters].
[55]For a review, see R.O. Jones and O. Gunnarsson, Rev. Mod. Phys. **61**, 689 (1989).
[56]R.O. Jones and D. Hohl, J. Chem. Phys. **92**, 6710 (1990) [P_n clusters].
[57]R.O. Jones and D. Hohl, J. Am. Chem. Soc. **112**, 2590 (1990) [Se_xS_y molecules].
[58]D. Hohl, R.O. Jones, R. Car, and M. Parrinello, J. Am. Chem. Soc. **111**, 825 (1989) [S_7O].
[59]R.O. Jones and D. Hohl, Proceedings of the 10th General Meeting of the Condensed Matter Division, European Physical Society, Lisbon, Portugal, 1990 [Phys. Scr. (to be published)].
[60]R.O. Jones and D. Hohl, Int. J. Quantum Chem., Symp. **24** (1990) [S_8, S_7O, O_8].
[61]S. Vosko, L. Wilk and M. Nusair, Can. J. Phys. **58**, 1200 (1980).
[62]T. Starkloff and J.D. Joannopoulos, Phys. Rev. B **16**, 5212 (1977).
[63]A. Lucas and B. Urbain, C. R. Acad. Sci. Paris **259**, 6403 (1964).
[64]R. Fischer and R.W. Schmutzler, in *The Physics of Selenium and Tellurium*, edited by E. Gerlach and P. Grosse (Springer, New York, 1979), p. 225.
[65]I. Štich, R. Car, M. Parrinello, and S. Baroni, Phys. Rev. B **39**, 4997 (1989).
[66]G. Etherington, A.C. Wright, J.T. Wenzel, J.C. Dore, J.H. Clarke, and R.N. Sinclair, J. Non-Cryst. Solids **48**, 265 (1982).
[67]D. Vanderbilt and J.D. Joannopoulos, Phys. Rev. B **27**, 6296 (1983); *ibid.* 6302 (1983); *ibid.* 6311 (1983).
[68]M. Springborg and R.O. Jones, J. Chem. Phys. **88**, 2652 (1988).
[69]B.W. Corb, W.D. Wei, and B.L. Averbach, J. Non-Cryst. Solids **53**, 29 (1982), and references therein.
[70]See, for example, R. Steudel, T. Sandow, and J. Steidel, Z. Naturforsch. Teil B **40**, 594 (1985).
[71]R.A. Street and N.F. Mott, Phys. Rev. Lett. **35**, 1293 (1975).
[72]M. Kastner, D. Adler, and H. Fritzsche, Phys. Rev. Lett. **37**, 1504 (1976).
[73]Requests concerning the visualization in this article can be e-mailed to dbock@ncsc.org. The software is available on request.

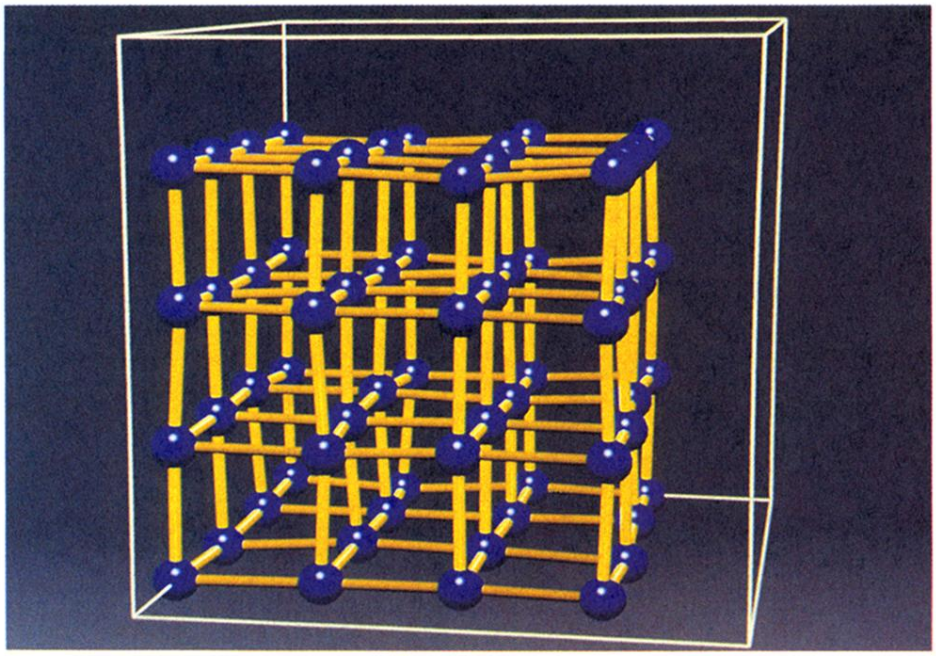

FIG. 1. Ball-and-stick model of the starting geometry used for the MD-DF simulation. 64 Se atoms were placed on randomly perturbed simple cubic lattice sites with the coordination number 6. The initial atomic spacing is ~6.1 a.u. Only atoms and bonds inside the periodically repeated cube are shown.

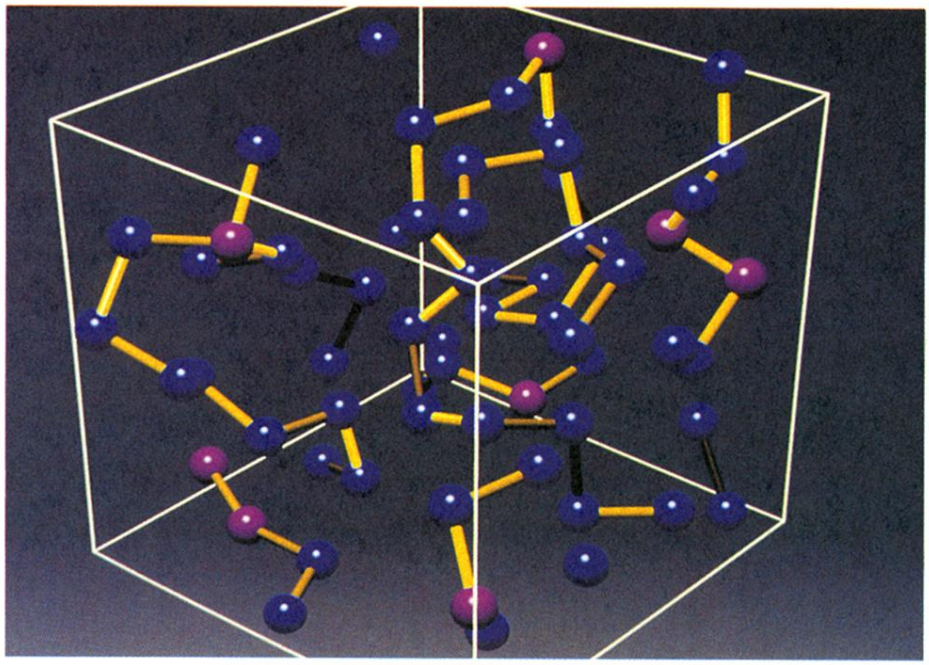

FIG. 8. Ball-and-stick model of a typical spatial configuration in amorphous selenium. All atoms inside the periodically repeated cube are shown and bonds are drawn between atoms within the cell with separation $d \leq 5.2$ a.u. Threefold coordinated atoms are shown in purple, all others in blue. Bonds to atoms in neighboring cells are omitted, so that the number of sticks is not necessarily a measure of the coordination number.

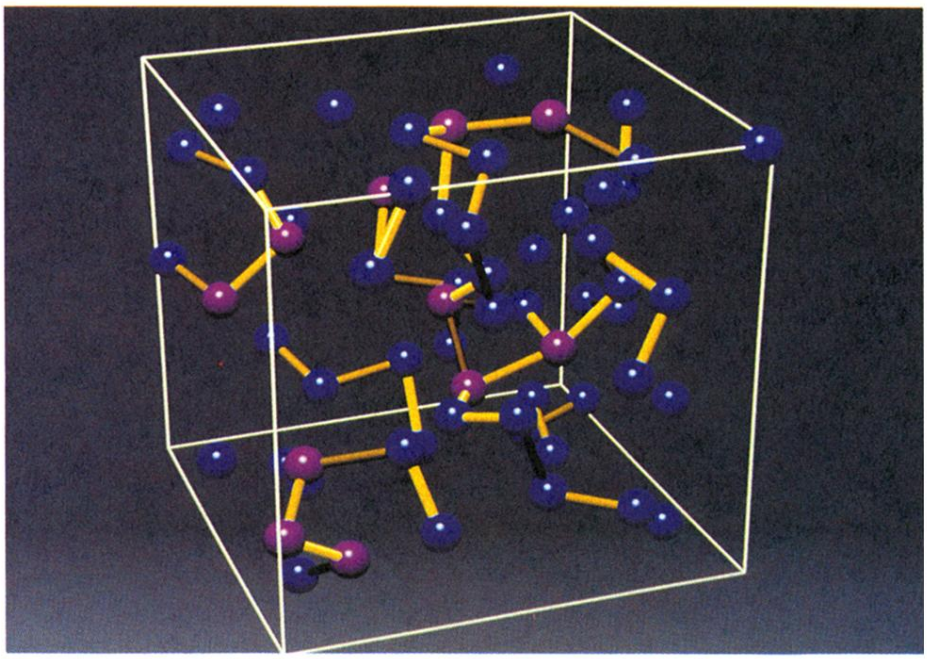

FIG. 9. Ball-and-stick model of a typical spatial configuration in liquid selenium. Threefold coordinated atoms cluster and are not as evenly distributed as in Fig. 8.